

基于 4-氨基-1,2,4-三唑和多金属氧酸盐为杂化配体的 Cu^{II}和 Cu^I配合物的水热合成及光催化性能

刘媛媛^{*,1,2} 张慧敏¹ 王鑫蕊¹ 丁 波¹ 刘正宇¹ 丁 斌^{1,2}

(¹天津师范大学化学学院,天津市功能分子结构与性能重点实验室,天津 300387)

(²南京大学配位化学国家重点实验室,南京 210093)

摘要: 在水热条件下,制备了 2 个基于多金属氧酸盐(POM)的 Cu^{II}和 Cu^I新型杂化配合物材料,即[Cu₂(4-NH₂-trz)₄(Mo₈O₂₆)(H₂O)₄]·5H₂O (**1**)和[Cu₄(4-NH₂-trz)₄Mo₈O₂₆] (**2**)(4-NH₂-trz=4-氨基-1,2,4-三唑)。通过单晶 X 射线衍射、傅里叶变换红外光谱和粉末 X 射线衍射分析确定了它们的结构。在配合物 **1** 中,4-氨基-1,2,4-三唑双齿配体连接 2 个相邻的 Cu^{II}中心形成双核结构单元,这些双核结构单元进一步通过 Mo₈O₂₆⁴⁻连接形成一维(1D)的杂化配位结构。在配合物 **2** 中,4-氨基-1,2,4-三唑双齿配体连接相邻 Cu^I中心构筑了独特的[Cu₄(4-NH₂-trz)₄]_n 一维螺旋链,这些左手和右手的一维螺旋链再通过(β-Mo₈O₂₆)⁴⁻连接形成 2D 杂化骨架。光催化实验研究表明,样品 **1** 和样品 **2** 对于不同有机染料(亚甲基蓝(MB)、罗丹明 B(RhB)和甲基橙(MO))具有很好的光催化降解能力。

关键词: 水热; Cu^{II}; Cu^I; 光催化; 有机染料

中图分类号: O614.43; O614.61+2

文献标识码: A

文章编号: 1001-4861(2018)04-0791-09

DOI: 10.11862/CJIC.2018.097

Hydrothermal Assembly and Photocatalytic Characterization of Polyoxometalate-Based Cu^{II} and Cu^I Hybrid Coordination Framework with 4-Amino-1,2,4-triazole

LIU Yuan-Yuan^{*,1,2} ZHANG Hui-Min¹ WANG Xin-Rui¹ DING Bo¹ LIU Zhen-Yu¹ DING Bin^{1,2}

(¹Key Laboratory of Inorganic-Organic Hybrid Functional Material Chemistry, Tianjin Normal University, Tianjin 300387, China)

(²State Key Laboratory of Coordination Chemistry, Nanjing University, Nanjing 210093, China)

Abstract: Under hydrothermal conditions, two novel polyoxometalate (POM)-based Cu^{II} and Cu^I hybrid materials, namely [Cu₂(4-NH₂-trz)₄(Mo₈O₂₆)(H₂O)₄]·5H₂O (**1**) and [Cu₄(4-NH₂-trz)₄Mo₈O₂₆] (**2**) (4-NH₂-trz=4-amino-1,2,4-triazole) have been designed and synthesized. Their crystal structures have been determined by single crystal X-ray diffraction, FT-IR infrared spectra and powder X-ray diffraction analysis. In **1**, bi-dentate 4-NH₂-trz ligands bridge two neighboring Cu^{II} centers forming dinuclear structural units, which are further linked by Mo₈O₂₆⁴⁻ ions and arranged into a one-dimensional (1D) hybrid coordination framework. In **2**, bidentate 4-NH₂-trz ligands also link neighboring Cu^I centers to generate unique 1D [Cu₄(4-NH₂-trz)₄]_n helical chains. Further these infinite right-hand and left-hand helical chains are linked by (β-Mo₈O₂₆)⁴⁻ anions to form a 2D hybrid framework. Photocatalytic activities for decomposition of different organic dyes (methylene blue (MB), rhodamine B (RhB) and methyl orange (MO)) have been investigated for **1** and **2**, indicating that **1** and **2** are good candidates for the photocatalytic degradation of these organic dyes. CCDC: 1554212, **1**; 1473507, **2**.

Keywords: hydrothermal; Cu^{II}; Cu^I; photocatalytic; organic dyes

收稿日期: 2017-12-13。收修改稿日期: 2018-01-07。

国家自然科学基金(No.21301128)、天津市自然科学基金(No.14JCQNJC05900)、天津市高等学校创新团队培养计划(No.TD12-5038)和天津师范大学大学生创新训练(No.201612)资助项目。

*通信联系人。E-mail: hxylyy@mail.tjnu.edu.cn

0 Introduction

In recent years, hybrid inorganic-organic complexes are a new generation of solid-state materials owing to their chemical and structural diversities^[1]. Polyoxometalates (POMs), a unique class of metal-oxide clusters, have been intensively investigated in many important aspects such as catalysis, electrical conductivity, medicine, magnetism, materials science, and biological chemistry^[2]. The wide application range is mainly based on (i) the ability of polyoxometalates to act as electron and proton reservoirs; and (ii) the extreme variability of their molecular properties including shape, size, acidity, and charge^[3]. Recently, many remarkable works about constructing metal-organic frameworks (MOFs) with desired properties is the use of the coordination ability of polyanions to combine with different transition-metal organic units have been presented in coordination polymers^[4-6]. This method may bring the merits of each row-material together, such as structural diversity and unique physical and chemical properties^[7].

For the construction of these POM-based CPs, the choice of organic ligands is very critical. The organic ligands can be subdivided into two classes: pre-synthesized and in situ synthesized ligands^[8]. The former have been used extensively in the POM-based reaction systems, including N-donor ligands, polycarboxylate ligands and so on^[9]. Among these Nitrogen-containing heterocyclic organic molecules, 1,2,4-triazole and its derivatives are interesting ligands because they combine the coordination geometries of both pyrazoles and imidazoles with regard to the arrangement of their three heteroatoms. For example, these organic linkers have been used to construct these open MOFs, which contain unsaturated metal clusters and possess high thermal stability and even framework flexibility^[10-11]. As the 1,2,4-triazole derivative, 4-amino-1,2,4-triazole (4-NH₂-trz) is a multi-dentate ligand containing one amino and one triazole group, which can provide strong nitrogen coordination donors to metal centers. It can be expected that 4-NH₂-trz ligand is able to be effectively imprinted onto

the metal coordination centers, affording versatile and structural tunable inorganic-organic POM-based hybrid materials^[12].

Previously we are also interested in exploiting the coordination chemistry and application of nitrogen-containing heterocyclic ligands and its derivatives^[13]. In this work, under hydrothermal conditions two novel Cu^{II} and Cu^I polyoxometalate (POM)-based hybrid materials, namely [Cu₂(4-NH₂-trz)₄(Mo₈O₂₆)(H₂O)₄]·5H₂O (**1**) and [Cu₄(4-NH₂-trz)₄Mo₈O₂₆] (**2**) have been designed and synthesized through simply tuning the molar ratio of reactant.

1 Experimental

1.1 General

All the reagents were purchased commercially and used without further purification. Deionized water was used as solvent in this work. The solvents were distilled from the appropriate drying agents prior to use. C, H and N microanalyses were carried out with a Perkin-Elmer 240 elemental analyzer. Elemental analysis (Mo) was performed on the X7 Series inductively coupled plasma mass spectrometer (ICP-MS) (Thermo Electron Corporation, U.S.A.). Powder X-ray diffraction analysis has been determined on a D/Max-2500 X-ray diffractometer using Cu K α radiation ($\lambda=0.154$ nm, $U=40$ kV, $I=40$ mA) with a 2θ range of $5^\circ \sim 50^\circ$. The UV-Vis diffuse reflectance spectra were obtained with a Lambda 900 UV-Vis-NIR spectroscopy at room temperature.

1.2 Preparation of coordination complexes **1** and **2**

1.2.1 [Cu₂(4-NH₂-trz)₄(Mo₈O₂₆)(H₂O)₄]·5H₂O (**1**)

A mixture of MoO₃ (0.086 g, 0.60 mmol), CuSO₄·5H₂O (0.051 g, 0.2 mmol), 4-NH₂-trz (0.016 g, 0.2 mmol) and H₂O (10 mL) ($n_{\text{Cu}}:n_{4\text{-NH}_2\text{-trz}}:n_{\text{MoO}_3}=2:2:6$) was heated at 160 °C for 72 hours under autogenous pressure, followed by cooling slowly ($5^\circ\text{C}\cdot\text{h}^{-1}$) to room temperature. Blue-green long shape crystals were isolated manually from blue unidentified powder, washed with water, and dried in air. Yield: 0.17 g (ca. 46% based on Cu). Anal. Calc. for C₈H₃₄Cu₂Mo₈N₁₆O₃₅ (%): C, 5.30; H, 0.19; N, 12.38; Mo, 42.43. Found(%):

C, 5.28; H, 0.15; N, 12.42; Mo, 42.45. IR (KBr, cm⁻¹): 3116 (bs), 2 675 (w), 1 517 (m), 1 425 (m), 1 305 (m), 1 025 (s), 903 (s), 825 (m), 606 (m).

1.2.2 [Cu₄(4-NH₂-trz)₄Mo₈O₂₆] (**2**)

A mixture of MoO₃ (0.057 g, 0.40 mmol), CuSO₄·5H₂O (0.076 g, 0.3 mmol), 4-NH₂-trz (0.025 g, 0.3 mmol) and H₂O (10 mL) ($n_{\text{Cu}^{II}}:n_{4\text{-NH}_2\text{-trz}}:n_{\text{MoO}_3}=4:3:3$) was heated at 160 °C for 72 hours under autogenous pressure, followed by cooling slowly (5 °C·h⁻¹) to room temperature. Red block crystals were isolated manually from blue unidentified powder, washed with water, and dried in air. Yield: 0.19 g (ca. 35% based on Cu). Anal. Calc. for C₈H₁₆Cu₄Mo₈N₁₆O₂₆ (%): C, 5.40; H, 0.90; N, 12.62; Mo, 43.27. Found (%): C, 5.38; H, 0.92; N, 12.72; Mo, 43.18. IR (cm⁻¹): 3 104 (m), 1 631 (m), 1 580 (m), 1 480 (m), 1 357 (w), 1 210 (w), 1 108 (s), 995 (s), 902 (m), 814 (m), 582 (m).

1.3 Photocatalytic measurements of coordination complexes **1** and **2**

The photocatalytic measurements of coordination polymers **1** and **2** were evaluated by the degradation of methylene blue (MB), rhodamine B (RhB) and methyl orange (MO) under irradiation of a 300 W high pressure mercury lamp. The experiments were carried out in typical processes, 5 mg complexes **1** and **2** were dispersed in aqueous solutions of three dyes (1×10^{-5} mol·L⁻¹, 10 mL), respectively. The mixture was stirred in the dark for 30 min for the adsorption-desorption equilibrium, then the mixture was transferred and placed under the lighting of Hg lamp (200 W) with continuous stirring. Next, every 20 min intervals, aliquots of the mixture samples were taken

out and centrifuged. Finally, the sample was analyzed by UV-Vis measurement. The degradation efficiency (*D*) of dye is defined as follow:

$$D = [(A_0 - A_t) / A_0] \times 100\% = [(C_0 - C_t) / C_0] \times 100\%$$

where *C*₀ and *A*₀ represents the initial concentration and absorbance of dyes solution after 30 min in the dark, *C*_{*t*} and *A*_{*t*} represents the concentration and absorbance of the dye at time *t*.

1.4 X-ray crystallography

Structure measurements of complexes **1** and **2** were performed on a computer controlled Bruker SMART 1000 CCD diffractometer equipped with graphite-monochromated Mo *K*α radiation with radiation wavelength 0.071 073 nm by using the ω-scan technique. The structures were solved by direct methods and refined with the full-matrix least-squares technique using the SHELXS-97 and SHELXL-97 programs^[14-15]. Anisotropic thermal parameters were assigned to all non-hydrogen atoms. The organic hydrogen atoms were generated geometrically; the hydrogen atoms of the water molecules were located from difference maps and refined with isotropic temperature factors. Analytical expressions of neutral-atom scattering factors were employed, and anomalous dispersion corrections were incorporated. Crystal data collection and refinement details for complexes **1** and **2** are summarized in Table 1. Selected bond lengths and angles for complexes **1** and **2** are listed in Table 2. Hydrogen bonds analysis was carried out using the PLATON program^[16], all the hydrogen bonds distances and angles are listed in Table S1.

CCDC: 1554212, **1**; 1473507, **2**.

Table 1 Crystal data and structure refinement information for complexes **1** and **2**

Complexes	1	2
Empirical formula	C ₈ H ₁₆ Cu ₄ Mo ₈ N ₁₆ O ₃₅	C ₈ H ₁₆ Cu ₄ Mo ₈ N ₁₆ O ₂₆
Formula weight	1 809.1	1 774.04
Crystal system	Triclinic	Triclinic
Space group	<i>P</i> $\bar{1}$	<i>P</i> $\bar{1}$
<i>a</i> / nm	1.033 59(17)	0.910 30(12)
<i>b</i> / nm	1.108 02(19)	1.076 06(14)
<i>c</i> / nm	1.235 1(2)	1.140 61(14)
α / (°)	69.953(3)	102.847(2)
β / (°)	67.181(3)	112.757(2)

Continued Table 1

$\gamma / (^{\circ})$	63.219(3)	108.449(2)
V / nm^3	1.139 4(3)	0.898 2(2)
Z	2	2
$F(000)$	868	836
$D_c / (\text{Mg} \cdot \text{m}^{-3})$	2.637	3.280
μ / mm^{-1}	3.153	5.119
Data, restraints, parameter	6 652, 4 653, 324	6 819, 4 466, 283
GOF	1.065	1.042
$R_1^a [I \geq 2\sigma(I)]$	0.029 7	0.036 9
wR_2^a (all data)	0.070 3	0.086 3

$$^a R_1 = \sum \|F_o\| - \|F_c\| / \sum \|F_o\|; wR_2 = [\sum w(F_o^2 - F_c^2)^2 / \sum w(F_o^2)^2]^{1/2}$$

Table 2 Selected bond lengths (nm) and angles ($^{\circ}$) for complexes **1** and **2**

Complex 1					
Cu(1)-O(14)	0.198 7(4)	Cu(1)-N(5)	0.203 5(4)	Cu(1)-N(1A)	0.198 9(4)
Cu(1)-O(15)	0.200 5(4)	Cu(1)-N(2) ⁱ	0.234 3(4)	Cu(1)-O(7)	0.235 3(3)
Mo(1)-O(4)	0.174 7(3)	Mo(1)-O(3)	0.189 4(3)	Mo(1)-O(1)	0.169 7(3)
Mo(1)-O(5) ⁱ	0.191 4(3)	Mo(1)-O(2)	0.217 3(3)	Mo(1)-O(5)	0.243 7(3)
O(14)-Cu(1)-N(1)	174.87(16)	O(14)-Cu(1)-O(15)	91.27(16)	N(1)-Cu(1)-O(15)	88.06(17)
O(14)-Cu(1)-N(5)	89.43(16)	N(1)-Cu(1)-N(5)	90.95(17)	O(15)-Cu(1)-N(5)	176.71(17)
O(14)-Cu(1)-N(2) ⁱ	84.09(15)	O(1)-Mo(1)-O(5)	179.15(16)	O(14)-Cu(1)-O(7)	87.23(13)
N(1)-Cu(1)-O(7)	87.83(14)	O(15)-Cu(1)-O(7)	97.99(14)	N(5)-Cu(1)-O(7)	78.84(14)
O(6)-Mo(2)-N(4)	93.86(16)	O(7)-Mo(2)-N(4)	80.82(15)	O(2)-Mo(1)-O(5)	164.35(15)
O(4)-Mo(1)-O(3)	146.55(14)	O(4)-Mo(1)-O(8)	77.08(13)	O(1)-Mo(1)-O(4)	103.97(17)
O(1)-Mo(1)-O(8)	158.38(17)	O(3)-Mo(1)-O(5)	70.52(12)		
Complex 2					
Cu(1)-N(1)	0.192 5(4)	Cu(3)-N(6)	0.188 7(4)	Mo(1)-O(8)	0.229 9(3)
Cu(2)-N(2)	0.187 6(4)	Mo(1)-O(1)	0.170 1(4)	Mo(1)-O(5)	0.237 1(3)
Cu(2)-N(5)	0.187 8(5)	Mo(1)-O(4)	0.191 7(3)	Mo(1)-O(3)	0.199 8(3)
N(2)-N(1)-Cu(1)	124.8(3)	O(1)-Mo(1)-O(2)	104.6(2)	O(3)-Mo(1)-O(8)	74.07(12)
N(2)-Cu(2)-N(5)	154.9(2)	O(1)-Mo(1)-O(4)	100.78(17)	O(1)-Mo(1)-O(5)	87.63(16)
N(6)-N(5)-Cu(2)	118.3(3)	O(2)-Mo(1)-O(3)	97.40(16)	O(2)-Mo(1)-O(5)	164.35(15)
O(4)-Mo(1)-O(3)	146.55(14)	O(4)-Mo(1)-O(8)	77.08(13)	O(4)-Mo(1)-O(5)	84.32(14)
O(1)-Mo(1)-O(8)	158.38(17)	O(3)-Mo(1)-O(5)	70.52(12)		

Symmetry code: ⁱ $x, 1.5-y, z+0.5$ for **1**; ⁱ $2-x, 2-y, -z$ for **2**.

2 Results and discussion

2.1 Preparations of coordination polymers **1** and **2**

The chemistry of copper(II)-molybdenum(VI) oxides itself represents a unique subclass of inorganic complex, in which the combination of different oxidation states, polyhedral types, and their

connectivity defines the structural variety of geometric forms^[17]. Coordination polymers **1** and **2** are stable in air and can retain their structural integrity at room temperature for a considerable long time. The successful isolation of complexes **1** and **2** relies on the exploitation of hydrothermal techniques. Hydrothermal reaction conditions are essential for preparing the final complexes **1** and **2**. On the other hand, complexes

1 and **2** are synthesized by using the same raw materials and similar hydrothermal synthetic conditions except only using different molar ratios ($n_{\text{Cu}^{\text{II}}}:n_{4\text{-NH}_2\text{-trz}}:n_{\text{MoO}_3}=2:2:6$ for **1** and $4:3:3$ for **2**). Therefore the molar ratios of reactants in the multi-component system were significant for the crystallization of products. In order to select the most appropriate hydrothermal reaction conditions to prepare these well-crystalline products **1** and **2**, different molar ratios of the reactants ($n_{4\text{-NH}_2\text{-trz}}/n_{\text{MoO}_3}$) varying from 2 to 6 are sequentially used, in which the molar quality of MoO₃ can vary from 0.2 to 0.6 mmol. The synthetic procedures for complexes **1** and **2** described in the experimental details were selected as the most appropriate ones. The different crystal structures of **1** and **2** show the important influence of the molar ratios of starting reagents.

In particular, as a d^9 metal, Cu^{II} ion can be easily converted into Cu^I ion in the presence of different types of reducer. The changeable oxidation states and versatile coordination geometries make copper ion can be used as a controllable linker. It is noted that Cu^{II} ion in complex **2** was reduced to Cu^I under hydrothermal conditions. Bond valence sum calculations for **1** and **2** show that all Mo atoms are in +6 oxidation state, while Cu atoms are in +1 oxidation state in **2** and the +2 oxidation state in **1**. Additionally, the oxidation state of the Cu atoms in **1** and **2** is further confirmed by their coordination environments and crystal color (blue-green long shape crystals for **1** and red block crystals for **2**).

2.2 Structural description

Single-crystal X-ray diffraction analysis reveals that complex **1** crystallizes both in $P\bar{1}$ space groups and triclinic crystal system. complex **1** consists of two Cu(II) ions, four 4-amino-1,2,4-triazol(4-atrz) ligands, one Mo₈O₂₆⁴⁻ anion, four coordinated water molecules and five interstitial water molecules. As shown in Fig. 1a, in complex **1**, 4-atrz ligands adopt pyrazolate-like [N-N]-bidentate bridging coordination mode. The Cu^{II} center (Cu1) is six-coordinated by three N atoms (N1A, N2 and N5) from triazolyl groups and three Oxygen atoms (O7, O14 and O15). These Oxygen

atoms O(14), O(15) act as the terminal coordinated water molecules, while the oxygen atom O(7) come from Mo₈O₂₆⁴⁻ anions further linked Cu1 atoms. Two six-coordinated Cu(II) atoms (Cu1 and Cu1A) are linked by two bi-dentate 4-atrz ligands forming binuclear Cu^{II} structural units. Further the dual-core structural units are linked by Mo₈O₂₆⁴⁻ ions through bridging O7 atom, which are arranged into the 1D hybrid metal-organic framework along the crystallographic *b* axis (Fig.1b). Numerous N-H···O and O-H···O hydrogen-bonding interactions (N(7)-H(7A)···O(1), 0.305 7(7) nm; N(7)-H(7B)···O(10), 0.300 5(6) nm; O(14)-H(14A)···O(16), 0.269 8(6) nm; O(15)-H(15A)···O(17), 2.681(7) nm; O(16)-H(16A)···O(11), 0.279 5(6) nm) also can be observed in the coordination framework of **1**, which also further extend **1** into a 3D supra-molecular network (Fig.1c).

Single-crystal X-ray diffraction analysis reveals that complex **2** also crystallizes in $P\bar{1}$ space groups and triclinic crystal system. Complex **2** consists of four Cu(I) ions (Cu1, Cu2, Cu2A and Cu3), four 4-amino-1,2,4-triazol(4-atrz) ligands and one Mo₈O₂₆⁴⁻ anion. As shown in Fig.2a, in complex **2**, Cu(1) is six-coordinated by two triazole nitrogen atoms and four oxygen atoms from Mo₈O₂₆⁴⁻ anions forming the octahedral coordination mode, Cu3 is four-coordinated by two triazole nitrogen atoms and two oxygen atoms from Mo₈O₂₆⁴⁻ anions forming the planar coordination mode while Cu2 are four-coordinated by two triazole nitrogen atoms (N2 and N5) and two polyoxometalate oxygen atoms forming the tetrahedral coordination geometry. These 4-atrz ligands bridge neighboring Cu^I centers forming tetra-nuclear Cu^I structural unit. It is interestingly that, as shown in Fig.2b, 1D [Cu₄(4-NH₂-trz)₄] helical chains can be observed, in which these Cu^I centers are extended by these bridging 4-atrz ligands. For **2**, these 1D right-hand and left-hand helical chains are linked by (β -Mo₈O₂₆)⁴⁻ anions to form the 2D hybrid framework of **2** (Fig.2c). These C-H···O, N-H···O and O-H···N hydrogen bonding interactions (N(4)-H(4A)···O(10), 0.320 95(4) nm; O(2W)-H(2A)···N(7), 0.280 8(6) nm; N(8)-H(8A)···O(10), 0.315 41(4) nm; N(8)-H(8B)···O(4), 0.297 13(4)

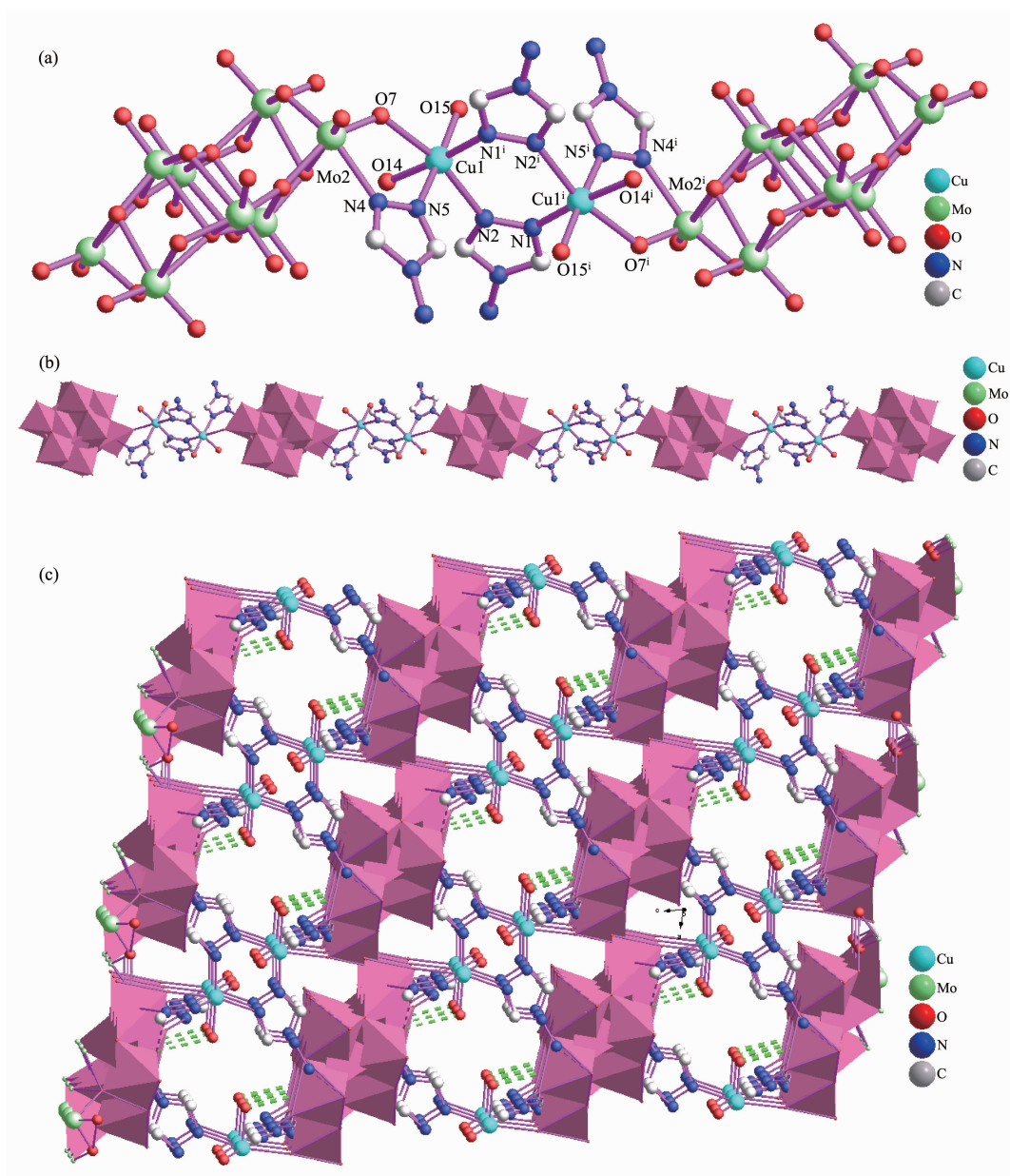


Fig.1 (a) Binuclear Cu^{II} structural units of **1** with H atoms are omitted for clarity; (b) Binuclear Cu^{II} structural units extended by $\text{Mo}_8\text{O}_{26}^{4-}$ ions forming the 1D hybrid metal-organic framework of **1**; (c) 3D supramolecular framework viewed along the b -axis direction (dashed lines represent hydrogen bonding interactions)

nm; $\text{C}(1)\cdots\text{O}(9)$, 0.319 13(4) nm) further extend 2D hybrid framework of **2** to generate a 3D supramolecular architecture (Fig.2d).

2.3 Powder X-ray diffraction (PXRD) and FT-IR characterizations

PXRD patterns of **1** and **2** are also recorded at room temperature to determine the phase purity. As shown in Fig.3, the positions of the experimental patterns are in good agreement with those of the simulated patterns, implying phase the as-synthesized

samples of **1** and **2** are pure. The slight differences in reflection intensities between the simulated and the experimental patterns are due to the variation in the crystal orientation of the powder sample.

In coordination complexes **1** and **2**, the FT-IR bands at 903, 825 cm^{-1} for **1** and 902, 814 cm^{-1} for **2** can be assigned to $\nu(\text{Mo}-\text{O})$ and $\nu(\text{Mo}-\text{O}-\text{Mo})$. FT-IR spectra also display typical characteristic absorption bands for triazole moieties of **L**. The peaks around $ca.$ 3 100 cm^{-1} and peaks located at 1 100~1 300 cm^{-1} ,

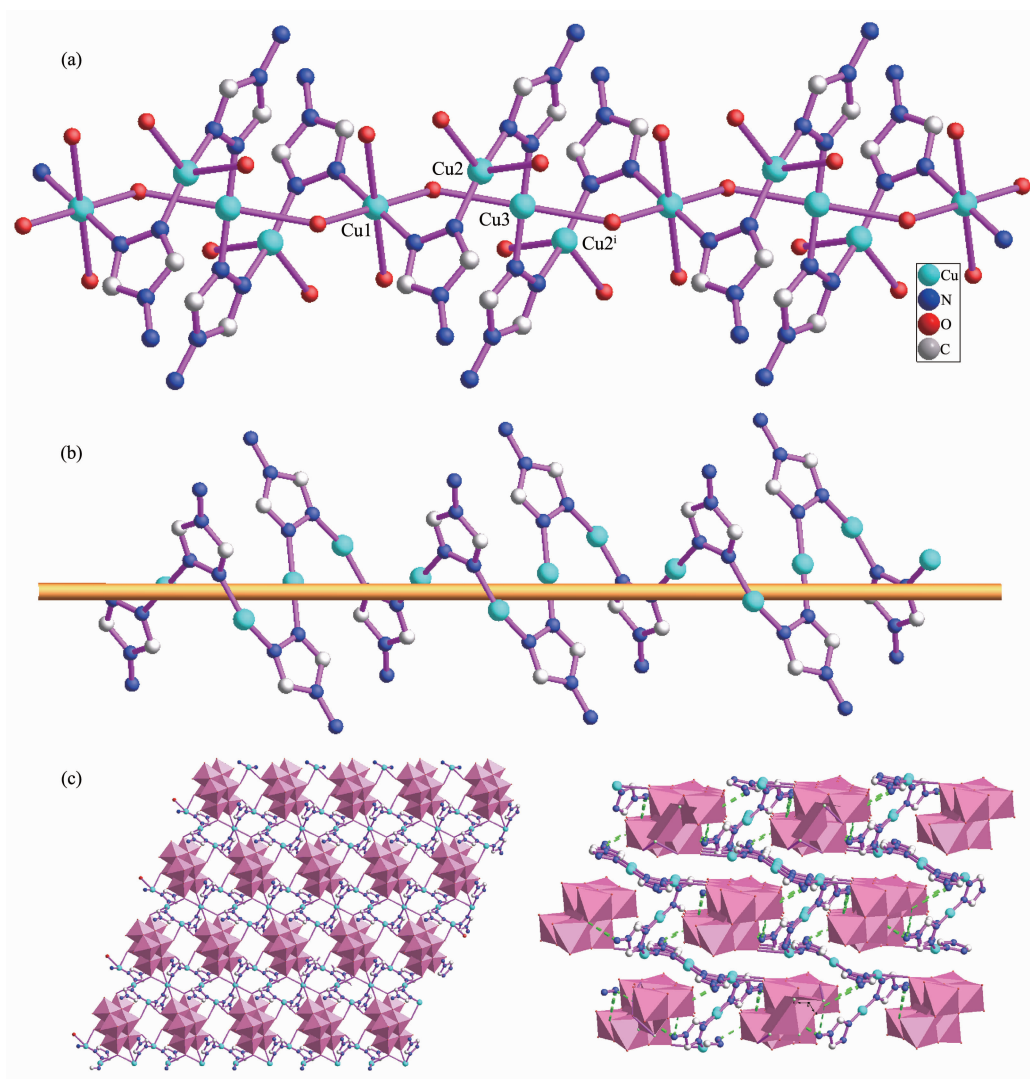


Fig.2 (a) Tetra-nuclear Cu^I structural unit in **2** with H atoms omitted for clarity; (b) 1D [Cu₄(4-NH₂-trz)₄] helical chains with Cu^I centers bridged by 4-amino-triazole ligands; (c) 1D right-hand and left-hand helical chains linked by (β-Mo₈O₂₆)⁴⁻ anions to form the 2D hybrid framework of **2**; (d) 3D supramolecular framework viewed along the crystallographic *b*-axis direction (dashed lines represent hydrogen bonding interactions)

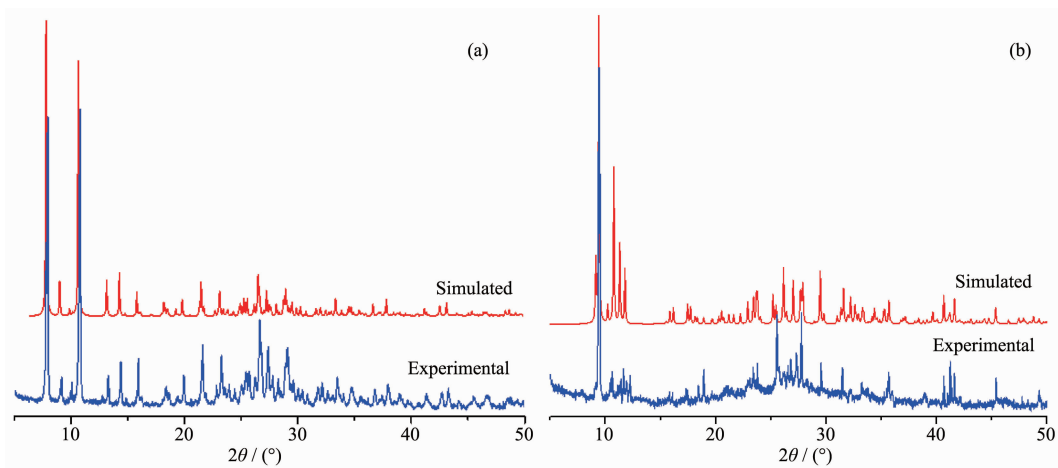


Fig.3 PXRD patterns for coordination framework (a) **1** and (b) **2**

which can be related to $\nu(\text{C-H})$ and $\nu(\text{C-N})$ or $\nu(\text{N-N})$ of triazole moieties. The triazole out of plane ring absorption is also observed at around 600 cm^{-1} (606 cm^{-1} for **1** and 582 cm^{-1} for **2**)^[18].

2.2 Photocatalytic capability for organic dyes of **1** and **2**

As our knowns, large numbers of commercial organic dyes are devoted to our daily life, however, they are also toxic and carcinogenic to us. Therefore how to rational utilize and purified the waste water can be the burning question to solve. Some reported about coordination polymers can show excellent photocatalytic capability in the degradation of organic dyes under UV irradiation^[19-20].

The photocatalytic activity of **1** and **2** in three different dye solutions is shown in Fig.4 and Fig.5. The entire six absorbance decrease obviously, moreover, the variation trend of the concentration ratios of the dyes (C_t/C_0) against time (t) with **1** in solutions were plotted, with C_0 representing the initial concentration of dyes after stirred in the dark for 20 min. As depicted in Fig.4, complex **1** shows remarkable photocatalytic capacity for these three organic dyes, and could be nearly completely degraded (the degradation efficiency (D) of dye is 99.4% for MB, 98.8% for RhB, and 84.6% for MO) in 100 min. Complex **2** also shows photocatalytic capacity for the three organic dyes, and could be nearly completely degraded (the degradation efficiency (D) of dye is 95.8% for MB, 96.8% for RhB, and 83.2% for MO) in 100 min. The results indicate that both complexes **1** and **2** could be an excellent

candidate for photocatalytic activity in the photocatalytic degradation of some organic dyes.

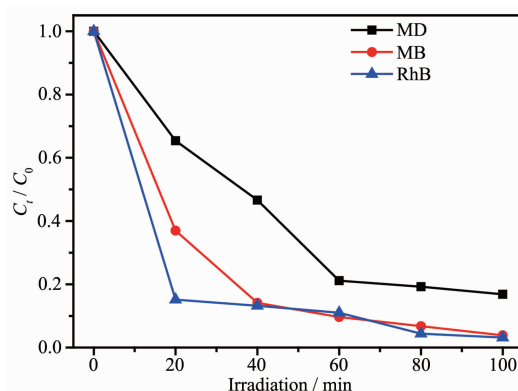


Fig.5 Plots of C_t/C_0 against irradiation time of MB, RhB and MO with coordination polymer **2**

With a view to the coordination environment, the kinds of the central metal ions and the coordinated mode of the ligand have significant influence on the photocatalytic activities. As described in the previous literature^[21-22], during the photocatalytic process of POM-based coordination polymers, UV-Vis light can induce POM/organic ligands to produce oxygen and/or nitrogenmetal charge transfer by promoting an electron from the highest occupied molecular orbital (HOMO) to the lowest unoccupied molecular orbital (LUMO). The HOMO strongly demands one electron to return to its stable state. Therefore, one electron is captured from water molecules, which are oxygenated into the $\cdot\text{OH}$ active species, which can decompose certain dyes thus effectively to complete the photocatalytic process^[23-24].

3 Conclusions

In summary, under similar hydrothermal conditions, only using different molar ratio for the stating materials ($n_{\text{Cu}^{\text{II}}}:n_{4\text{-NH}_2\text{-trz}}:n_{\text{MoO}_3}=2:2:6$ for **1** and $4:3:3$ for **2**), two novel polyoxometalate (POM)-based Cu^{II} and Cu^{I} hybrid materials, namely $[\text{Cu}_2(4\text{-NH}_2\text{-trz})_4(\text{Mo}_8\text{O}_{26})(\text{H}_2\text{O})_4] \cdot 5\text{H}_2\text{O}$ (**1**) and $[\text{Cu}_4(4\text{-NH}_2\text{-trz})_4\text{Mo}_8\text{O}_{26}]$ (**2**) ($4\text{-NH}_2\text{-trz}=4\text{-amino-1,2,4-triazole}$) have been designed and synthesized. Their crystal structures have been determined by single crystal X-ray diffraction, FT-IR infrared spectra and powder X-ray diffraction. PXRD patterns of the bulky samples **1** and **2** also

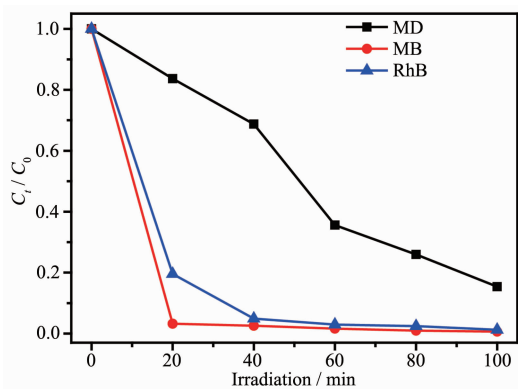


Fig.4 Plots of C_t/C_0 against irradiation time of MB, RhB and MO with coordination polymer **1**

have been determined, which agree well with theoretical PXRD patterns confirming pure phases. Photocatalytic activities for decomposition of different organic dyes have been investigated for complexes **1** and **2**, indicating that **1** and **2** have significant photocatalytic degradation effect to these organic dye molecules. The result also reveals that great potential in the construction of these novel metal organic frameworks employing different triazole derivatives and versatile polyoxometalate (POM)-based building blocks. On the basis of this work, further syntheses, structures and properties studies of these coordination polymers using these versatile building blocks are also under way in our laboratory.

Supporting information is available at <http://www.wjhxxb.cn>

References:

- [1] Banerjee R, Phan A, Wang B, et al. *Science*, **2008**,**319**:939-943
- [2] Anjass M H, Kastner K, Nagele F, et al. *Angew. Chem. Int. Ed.*, **2017**,**56**:14749-14752
- [3] Yi X F, Izarova N V, Stuckart M, et al. *J. Am. Chem. Soc.*, **2017**,**139**:14501-14510
- [4] Zhang Z M, Duan X P, Yao S, et al. *Chem. Sci.*, **2016**,**7**:4220-4229
- [5] Fu H, Qin C, Lu Y, et al. *Angew. Chem. Int. Ed.*, **2012**,**51**:7985-7989
- [6] Zhu S L, Xu X, Ou S, et al. *Inorg. Chem.*, **2016**,**55**:7295-7300
- [7] Chen L Y, Luque R, Li Y W, et al. *Chem. Soc. Rev.*, **2017**, **46**:4614-4630
- [8] Zhu P P, Sun L J, Sheng N, et al. *Cryst. Growth Des.*, **2016**, **16**:3215-3223
- [9] Li X X, Wang Y X, Wang R H, et al. *Angew. Chem. Int. Ed.*, **2016**,**55**:6462-6466
- [10] Haasnoot J G. *Coord. Chem. Rev.*, **2000**,**200-202**:131-185
- [11] Li X X, Xu H Y, Kong F Z, et al. *Angew. Chem. Int. Ed.*, **2013**,**52**:13769-13773
- [12] Zhu P P, Sheng N, Li M T, et al. *J. Mater. Chem. A*, **2017**, **5**:17920-17925
- [13] Ding B, Wang Y Y, Liu S X, et al. *CrystEngComm*, **2015**, **17**:5396-5409
- [14] Sheldrick G M. *SHELXS-97, Program for X-ray Crystal Structure Solution*, University of Göttingen, Germany, **1997**.
- [15] Sheldrick G M. *SHELXL-97, Program for X-ray Crystal Structure Refinement*, University of Göttingen, Germany, **1997**.
- [16] Spek A L. *J. Appl. Crystallogr.*, **2003**,**36**:7-13
- [17] Senchyk G A, Lysenko A B, Domasevitch K V, et al. *Inorg. Chem.*, **2017**,**56**:12952-12966
- [18] Fiher M E. *Am. J. Phys.*, **1964**,**32**:343-345
- [19] Wang X L, Gong C H, Zhang J W, et al. *CrystEngComm*, **2015**,**17**:4179-4189
- [20] Cui J W, An W J, Kristof Van H, et al. *Dalton Trans.*, **2016**, **45**:17474-17484
- [21] Dolbecq A, Mialane P, Keita B, et al. *J. Mater. Chem.*, **2012**, **22**:24509-24521
- [22] HOU Bu-Wei (侯不唯), LI Kai (李恺). *Chinese J. Inorg. Chem.*(无机化学学报), **2017**,**33**(6):1007-1014
- [23] Hu J M, Blatov V A, Yu B Y, et al. *Dalton Trans.*, **2016**,**45**:2426-2429
- [24] Meng X M, Fan C B, Bi C F, et al. *CrystEngComm*, **2016**, **18**:2901-2912